ORIGINAL ARTICLE

Microphase-separated structure and mechanical properties of cycloaliphatic diisocyanate-based thiourethane elastomers

Rahmawati Rahmawati[1,2] · Shuhei Nozaki[1] · Ken Kojio [1,3,4] · Atsushi Takahara [1,3,4] · Naoki Shinohara[5] · Satoshi Yamasaki[5]

Abstract

Polythiourethane (PTU) and polyurethane (PU) elastomers were prepared from poly(oxytetramethylene) glycol, 1,4-bis (isocyanatomethyl) cyclohexane and a dithiol or diol chain extender with two methylene numbers (tetramethylene (C4) and pentamethylene (C5)). The effect of dithiol and diol and the methylene length of the chain extenders on the microphase-separated structure and mechanical properties of PTU and PU were evaluated. Differential scanning calorimetry (DSC) and wide-angle X-ray diffraction measurements revealed that the degree of ordering of hard segment chains in PTUs is lower than that for PU elastomers. However, it was revealed from the DSC, small-angle X-ray scattering and temperature dependent dynamic viscoelasticity measurements that the degree of microphase separation in the PTUs became stronger than that for the PUs. As a result, the mechanical property of PTUs is comparable with PUs. Furthermore, the glass transition temperature for the soft segment of PTU became lower than that for PU. PTU and PU exhibited a larger degree of microphase separation and mechanical property when the chain extender was composed of a tetramethylene (C4) chain compared to a pentamethylene (C5) chain.

Introduction

Polyurethane (PU) has been fascinating for more than 60 years. Recently, different types of polyurethane, such as, hydroxyl PU [1–4], phenolic PU [5], sulfur-containing PU

[6, 7], and inorganic filler—another polymer-containing PU [8], have been synthesized to improve PU properties. Polythiourethanes (PTUs) are members of the PU family, which can be obtained by the reaction between isocyanate and dithiol—instead of diol—as the chain extender. When polymer materials include sulfur atoms, the refractive index will be generally increased, resulting in materials with potential for optical application. Another expected and attainable property of sulfur-including materials is an adhesive property. Sulfur atoms can form strong bonds with a metal surface, and sometimes exhibit a good adhesive property. Therefore, there is an expectation that PTUs may possess some properties that PUs do not possess. Some researchers have reported on the physical properties of thiourethane [9–14]. Li et al. investigated a series of hard segment models for urethane, thiourethane, and dithiourethane compounds. They found that the hydrogen bond strength of urethane is somewhat similar to thiourethane, while dithiourethane shows a lower propensity for hydrogen bonding compared to the urethane and thiourethane. Their findings suggest that the hydrogen bond strength and fraction, and the structure of diisocyanate makes a contribution to the physical and mechanical properties of polyurethane, polythiourethane, and polydithiourethane [11]. In addition,

✉ Atsushi Takahara
takahara@cstf.kyushu-u.ac.jp

[1] Graduate School of Engineering, Kyushu University, Fukuoka, Japan

[2] Center for Isotope and Radiation Application, National Nuclear Energy Agency of Indonesia (BATAN), Jl. Lebak Bulus Raya No.49, Jakarta 12440, Indonesia

[3] Institute for Materials Chemistry and Engineering, Kyushu University, Fukuoka, Japan

[4] WPI-I2CNER, Kyushu University, 744 Motooka, Nishi-ku, Fukuoka 819-0395, Japan

[5] Synthetic Chemicals Laboratory, R&D Center, Mitsui Chemicals, 580-32, Nagaura, Sodegaura, Chiba 299-0265, Japan

Shin et al. studied the impact of phase separation on the mechanical properties of PTUs in terms of the hard and soft segment molecular weight and ratio, and the hard segment chemical structure. They found that the aforementioned factors have a strong influence on the Young's modulus, and elongation at break and tensile strength [12]. However, there are no reports on the effect of the dithiol and diol chain extender on the microphase-separated structure and mechanical properties.

The purpose of this study is to investigate the effect of dithiol and diol, and the methylene length of the chain extender on the microphase-separated structure and mechanical properties of PTU and PU elastomers using differential scanning calorimetry (DSC), small-angle X-ray scattering (SAXS), wide-angle X-ray diffraction (WAXD), dynamic viscoelastic property measurement, and tensile testing. To evaluate the effect of dithiol and diol, and the methylene length of the chain extender on the microphase-separated structure, dithiol and diol with two types of methylene length for the chain extender were used, which polymerized with poly(oxytetramethylene) glycol (PTMG) and 1,4-bis(isocyanatomethyl)cyclohexane (1,4-H_6XDI). Since the dithiol group has a different character compared to the diol group, there is the expectation that the elastomers obtained from this chain extender exhibit various properties that have not been obtained before.

Experimental section

Raw materials for PTUs and PUs

1,4-bis(isocyanatomethyl)cyclohexane (FORTIMO^{TM} 1,4-H_6XDI, produced by Mitsui Chemicals Inc.) and Poly (oxytetramethylene) glycol (PTMG: $M_n = 1800$, Asahi Kasei Chemicals Co., Ltd., Japan) were employed as the diisocyanate and polyol, respectively. 1,4-butanedithiol (BDT), 1,5-pentanedithiol (PDT), 1,4-butanediol (BD), and 1,5-pentanediol (PD) (FUJIFILM Wako Pure Chemicals Co., Ltd., Japan) were used as chain extenders, with a hard segment weight fraction of ~16%. All chain extenders were purified by distillation, whereas 1,4-H_6XDI was used without further purification.

Synthesis of polythiourethanes

The four segmented polythiourethane and polyurethane were prepared by a prepolymer method in bulk using PTMG, 1,4-H_6XDI and the chain extender. Figure 1 shows the synthetic scheme for PTU and PU.

The fractions of hard segment were ca. 16 wt%. PTMG was dried under reduced pressure with dry nitrogen. Prepolymers were synthesized from 1,4-H_6XDI and PTMG with the ratio of $K = [NCO]_{iso}/[OH]_{PTMG} = 1.40$, at 80 °C for 3 h under N_2 atmosphere. As a catalyst, dibutyltin dilaurate (DBTL, FUJIFILM Wako Pure Chemical Co., Ltd. Japan) was added. The extent of the prepolymer reaction was observed by using an amine equivalent method, and, then, stopped when the reaction ratio for the NCO groups reached over 90%. To remove the air inside, the obtained prepolymer was degassed in vacuum. The chain extender was added to the prepolymer with a ratio of $[NCO]_{pre}/[SH] = 1.02$, where $[NCO]_{pre}$ is the number of moles of NCO groups in the prepolymer and [SH] is the number of moles of SH groups. After agitating, the product was poured into a mold consisting of two aluminum plates with a 2-mm-thick spacer and heated at 110 °C for 24 h to perform polymerization.
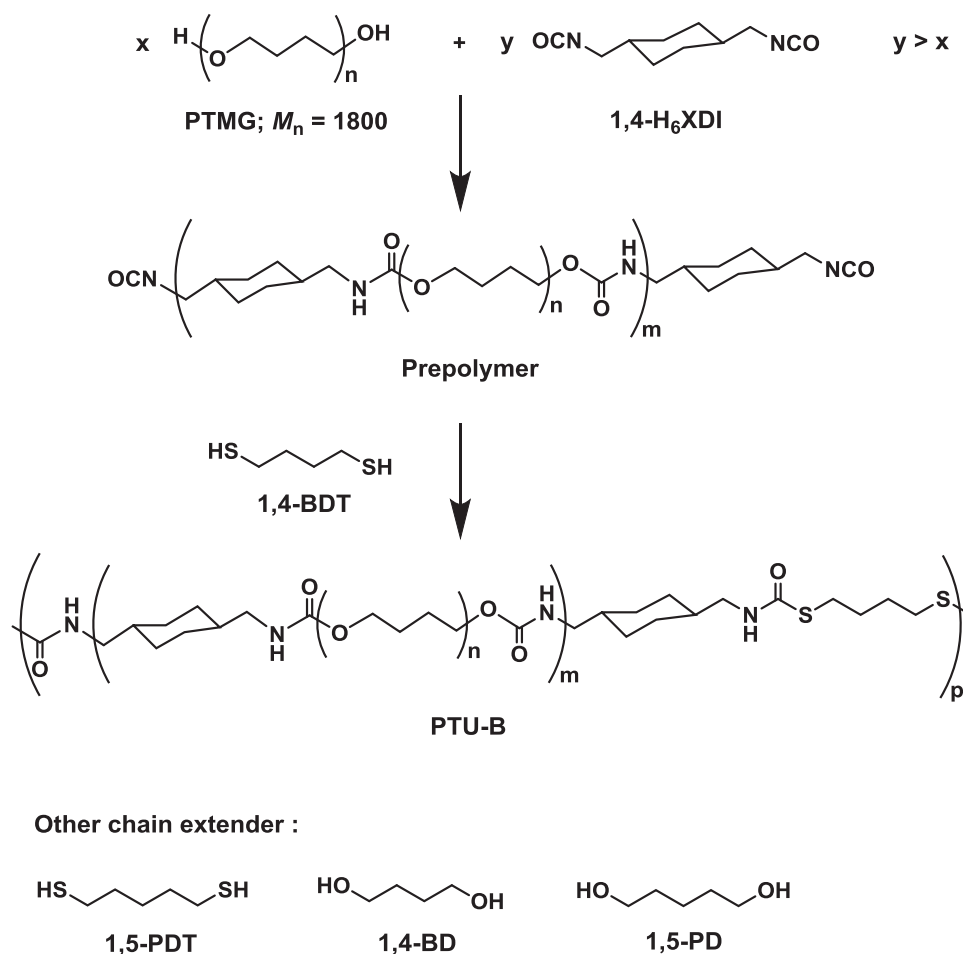
Characterization

To investigate the network structure of PTU and PU, the gel fraction and the degree of swelling were evaluated. N,N-dimethylacetamide (DMAc) and toluene were used as polar and non-polar solvent, respectively. The gel fraction, G, was defined as $G = W_b/W$, where W is the initial weight, and W_b is the dried weight after swelling with a solvent. The degree of swelling, Q, was defined as $Q = 1 + [(W_a - W_b)/d_s/(W_b/d_p)]$, where W_a, d_s, and d_p is the weight of the samples swollen to an equilibrium state, density of the solvent and density of the elastomers, respectively.

A Fourier transform infrared (FT-IR) spectroscopic measurement was conducted to evaluate the hydrogen bond state for the hard segment. A Spectrum One FT-IR spectrometer (PerkinElmer), Mercury cadmium telluride (MCT) detector, and attenuated total reflectance (ATR) accessory (Ge crystal, 45°) were employed for measurements. All FT-IR spectra were acquired at a resolution of 4 cm^{-1} with 32 scans.

Differential scanning calorimetric (DSC) thermograms were obtained using a DSC (DSC6220, SII EXSTAR 6000, Seiko Instruments) from −140 to 240 °C with a heating rate of 10 °C min^{-1} under a N_2 atmosphere.

The molecular aggregation structure was evaluated by synchrotron radiation X-ray analyses at the Frontier Soft-material Beamline (FSBL, BL03XU) in the SPring-8 facility in Japan [15, 16]. Simultaneous wide-angle X-ray diffraction (WAXD) and small-angle X-ray scattering (SAXS) measurements can be conducted in this beamline. The wavelength and size of the X-ray beam was 0.1 nm and 150 μm × 150 μm. A PILATUS 1M (DECTRIS, Ltd., pixel size of 172 μm) was used to obtain scattering in the small-angle region with a camera length of ca. 4 m. A flat panel detector was employed for WAXD measurements with a camera length of 74 mm. Scattering patterns were measured with an exposure time of 200–500 ms. The data were processed using the FIT-2D (Ver. 12.077, Andy Hammersley/ ESRF, Grenoble, France).

Fig. 1 Reaction scheme for PTU-B using a prepolymer method

PTMG; M_n = 1800

1,4-H$_6$XDI

y > x

Prepolymer

1,4-BDT

PTU-B

Other chain extender :

1,5-PDT   1,4-BD   1,5-PD

Temperature dependence of dynamic viscoelastic functions were obtained with a dynamic viscoelastometer (RHEOVIBRON DDV-01FP, ORIENTEC). Measurements were performed from −145 to 240 °C with a heating rate of 1 °C min^{-1} under N$_2$ atmosphere. The dimension of the specimens used was 30 mm × 5 mm × 0.3 mm. The applied frequency was 11 Hz.

Tensile testing was carried out with EZ-Graph (Shimadzu, Japan) at room temperature. The dimension of the samples was 100 mm × 5 mm × 2 mm. The initial length and elongation rate were 30 mm and 10 mm min^{-1}, respectively.

Results and discussion

Abbreviation denotes the type of polymer and chain extender. Table 1 shows the basic properties including degree of swelling, density, and gel fraction of the PTU and PU elastomers. All samples were soluble in dimethylacetamide (DMAc), indicating the existence of only physical crosslinks that undergo dissociation in the polar solvent. The gel fraction of elastomers prepared using a BD-based

Table 1 Basic properties of the PTU and PU elastomers

Sample	Density (g cm^{-3})	Gel fraction, G (%)		Degree of swelling, Q	
		Toluene	DMAc	Toluene	DMAc
PTU-B	1.02	98.5 ± 0.3	Soluble	2.23 ± 0.05	Soluble
PTU-P	1.02	71.7 ± 0.5	Soluble	2.82 ± 0.04	Soluble
PU-B	1.02	99.3 ± 0.4	Soluble	2.16 ± 0.03	Soluble
PU-P	1.02	79.4 ± 0.3	Soluble	2.81 ± 0.04	Soluble

chain extender swollen by toluene were ~99%, implying that the physical crosslinking network is well-developed. Moreover, the degree of swelling in toluene for elastomers with PD-based chain extenders is larger than that for BD-based chain extenders, suggesting less ordered hard segment chains. The influence of the methylene length of the chain extender on the degree of swelling for PU is stronger than that for PTU.

The hydrogen bonding state for the PTU and PU elastomers was assessed by ATR-FTIR analysis (Figure S1). The stretching vibrations of the NH groups and carbonyl bands indicate the presence of thiourethane and urethane

moieties. The NCO stretching band at $2260 \, \text{cm}^{-1}$ was not observed in all spectra, indicating that the reaction occurred properly. Absorption bands at ~1722, 1705, and $1688 \, \text{cm}^{-1}$ correspond to urethane carbonyl free ($v(C=O)_{U\text{-free}}$), disordered and ordered hydrogen-bonded carbonyl groups of urethane ($v(C=O)_{U\text{-H-bond}}$) stretching vibrations, respectively [17]. Whereas thiourethane carbonyl free ($v(C=O)_{TU\text{-free}}$) and hydrogen-bonded carbonyl groups of thiourethane ($v(C=O)_{TU\text{-H-bond}}$) stretching vibrations appear at ~1670–1640 cm^{-1} [18–20]. The NH stretching regions at ~3450, 3290–3310, and 3300–3350 cm^{-1} are assigned to urethanes NH free ($v(NH)_{free}$), hydrogen-bonded NH groups with ether oxygen ($v(NH)_{ether}$) of PTMG and urethane carbonyl groups ($v(NH)_{U\text{-carbonyl}}$) stretching vibrations, respectively [21, 22]. In addition, the bands at approximately 3301–3332 cm^{-1} arise from the hydrogen-bonded NH moiety of the thiourethane group ($v(NH)_{TU\text{-H-bond}}$) [11, 18].

Figure 2 shows DSC thermograms for the PTU and PU elastomers. For all samples, a baseline shift was observed at approximately $-72 \, °C$. This can be assigned to the glass transition temperatures of the soft segment chains ($T_{g,S}$) for the PTUs and PUs. The $T_{g,S}$ value for the PTUs is slightly lower than that for PUs, indicating that the PTUs possess a stronger degree of microphase separation. It is well-known that an increasing $T_{g,S}$ for PU elastomers is a consequence of increasing phase mixing. An exothermic peak corresponding to reorganized crystallization of activated PTMG chains and an endothermic peak being assignable to the melting of crystallized PTMG chains ($T_{m,S}$) were measured at approximately -36 to -27 and -4 to $10 \, °C$, respectively.

Exothermic peaks for the PTUs were larger than those for the PUs because of the difficulty of reorganized crystallization of the soft segments during the heating process [23–25]. In contrast, the soft segment in the PUs can easily
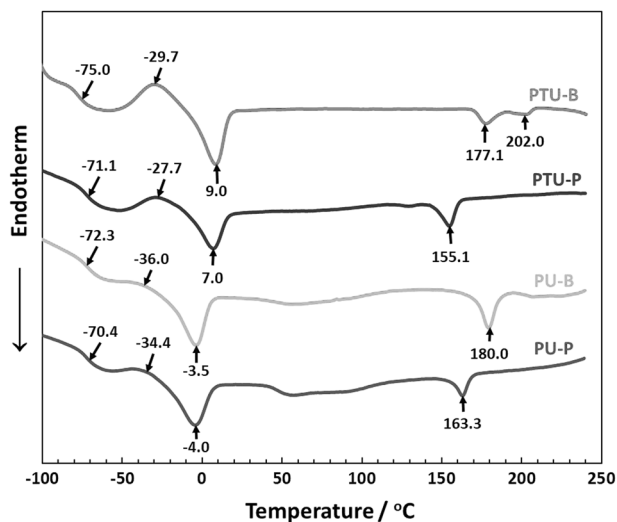
crystallize with the cooling process. Furthermore, PTUs showed a lower melting temperature ($T_{m,H}$) compared to the PUs, indicating that the ordering and lamella thickness of the hard segment of the PTUs are lower and smaller than for PUs, respectively. In addition, elastomers with a PD-based chain extender show a lower $T_{m,H}$ in comparison with elastomers with the BD-based chain extender. This is due to the lack of molecular symmetry, curved molecules, and relatively large distances of the hydrogen bond in elastomers with a PD-based chain extender [26].

WAXD measurements were conducted to examine the hard segment crystal structures of the PTUs and PUs. Figure 3 exhibits WAXD profiles for the PTUs, PUs together with the related hard-segment models for comparison. The PTU-B showed a weak peak and shoulders at $q = 12.1$, 13.7, and $16.1 \, \text{nm}^{-1}$, which correspond well to the $-(1,4\text{-}H_6\text{XDI-BDT})_n-$ model. A weak peak and shoulders were also observed for PU-B at $q = 12.1$, 13.0, 13.8, 15.0, and $16.4 \, \text{nm}^{-1}$, which correspond well to peaks of the $-(1,4\text{-}H_6\text{XDI-BD})_n-$ model. These results suggest that there exist crystalline hard segment domains, consistent with the related hard segment model in PU-B. In contrast, the WAXD profile for PTU-P and PU-P only exhibited an amorphous halo at ~13.8 nm^{-1}. The crystalline peaks cannot be observed due to overlap with an amorphous halo of the soft segment [27, 28]. This result implies that the elastomers with a PD-based chain extender possess less ordered crystalline hard segment chains [29].
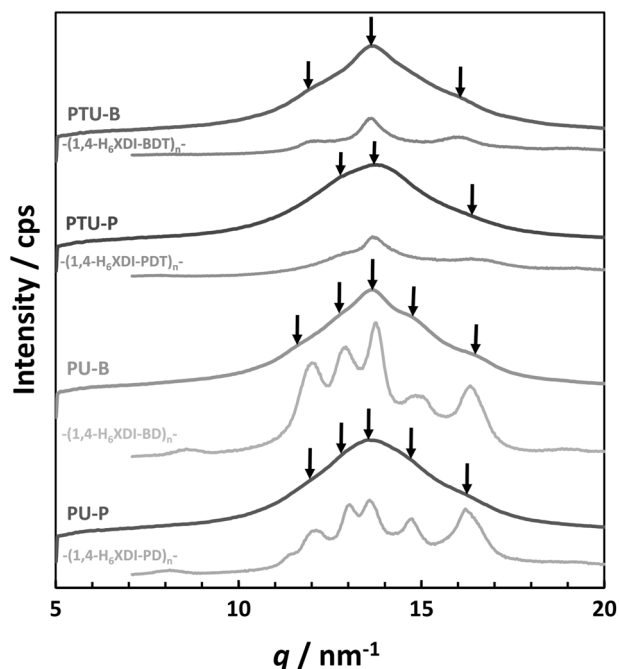

Fig. 2 DSC thermograms for the PTU and PU elastomers

Fig. 3 WAXD profiles for the PTUs, PUs, and the related hard-segment models

To obtain particular insight for the microphase-separated structure of PTU and PU elastomers, a SAXS measurement was conducted. Figure 4 shows the SAXS profiles and calculated three-dimensional correlation functions for the PTU and PU elastomers. Scattering peaks with a broad shape are observed in the q range 0.1–1.0 nm^{-1}. The peak is assigned to the spacing between hard segment domains in the microphase-separated system.

The spacing between hard segment domains was defined from analysis of three-dimensional correlations functions, γ_3 (r), from the following equation:

$$\gamma_3(r) = \frac{1}{Q} \int_0^\infty q^2 I(q) \frac{\sin(qr)}{qr} dq \tag{1}$$

The diffuse boundary thickness was obtained from Porod's law, with the quantitative analysis for the microphase separation evaluation determined by the calculation method proposed by Vonk [30], Bonart and Muller [31], and Koberstein and Stein [32].

The overall degree of phase separation for a complete phase separated two-phase system is defined as the ratio of the experimental electron density variance to the theoretical variance

$$\overline{\Delta\eta^{2\prime}} / \overline{\Delta\eta_c^2} \tag{2}$$

with the theoretical electron density variance assuming complete phase separation is defined as

$$\overline{\Delta\eta_c^2} = \emptyset_{HS}\emptyset_{SS}(\eta_{HS} - \eta_{SS})^2 \tag{3}$$

where $\emptyset_{HS}$ and η_{HS} are the volume fractions and electron densities of the hard segment, respectively.

The experimental electron density variance can be calculated from the background corrected intensities for one-dimensional scattering data using Porod's invariant Q

$$\overline{\Delta\eta^{2\prime}} = cQ = c \int_0^\infty [I(q) - I_b(q)]q^2 dq \tag{4}$$

with the effects of diffuse phase boundaries calculated from

$$\overline{\Delta\eta^{2\prime\prime}} = c \int_0^\infty \frac{[I(q) - I_b(q)]q^2}{H^2(q)} dq \tag{5}$$

where

$$c = \frac{1}{2\pi^2 i_e N_A^2} = 1.76 \times 10^{-24} \text{mol}^2/\text{cm}^2 \tag{6}$$

N_A is Avogadro's number, and i_e is Thompson's constant for the scattering from one electron. $H(q)$ is the function characterizing the shape and size of the interfacial boundary between two phases and $I_b(q)$ is the background intensity due to thermal density fluctuation. For a sigmoidal-shaped interface

$$H(q) = \exp\left(-\frac{\sigma^2 q^2}{2}\right) \tag{7}$$

and for a linear-gradient model

$$E \cong \sqrt{2\pi}\sigma \tag{8}$$

with $E = 0$ and $H(q) = 1$ for a sharp interface. σ is the width of the boundary layer whose value is obtained from the
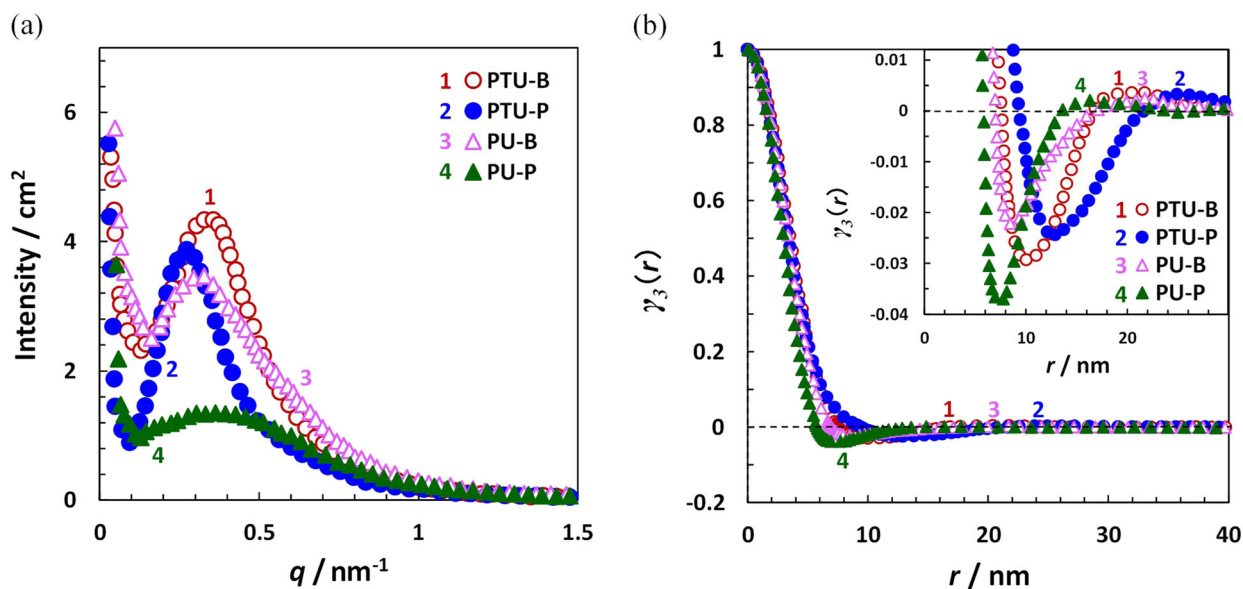

Fig. 4 a SAXS profiles and **b** calculated three-dimensional correlation functions for the PTU and PU elastomers

Table 2 The domain spacing, boundary thickness, and degree of microphase separation in the PTU and PU elastomers

Sample	Domain spacing obtained from Bragg's law/nm	Domain spacing obtained from three-dimensional correlation function/nm	Overall phase separation $(\Delta\eta^{2'}/\Delta\eta_c^2)$	Diffuse boundary mixing $(\Delta\eta^{2''}/\Delta\eta^{2'})$-1	Phase mixing within domains $(\Delta\eta_c^2/\Delta\eta^{2''})$-1	Thickness of diffuse microphase boundary/nm	
						Sigmoidal	Linear
PTU-B	18.6	20.2	0.35	0.02	1.76	0.19	0.46
PTU-P	23.5	25.2	0.26	0.03	2.67	0.21	0.52
PU-B	20.2	21.9	0.25	0.02	2.94	0.17	0.42
PU-P	15.1	15.7	0.17	0.03	4.85	0.17	0.43

The hard segment densities were obtained by modeling the crystal structure of hard segment models (Table S1, Figure S2, and S3).

The definition of phase boundary thickness is provided in the Supporting information (Figure S4).

scattering intensity calculated using Porod's law

$$I(q) = \frac{K_p}{q^4}\exp(-\sigma^2 q^2) + I_b(q) \qquad (9)$$

where K_p, σ, and I_b are estimated by fitting the scattering curves at large q values.

The obtained results can be seen in Table 2. PTUs exhibit a greater value of overall degree of microphase separation compared to PUs, which is influenced by both diffuse boundary mixing $(\Delta\eta^{2''}/\Delta\eta^{2'}) - 1$ and phase mixing within domains $(\Delta\eta_c^2/\Delta\eta^{2'}) - 1$. Although the diffuse boundary mixing is about the same, the contribution of phase mixing within domains leads to an obviously different value for the overall phase separation. In addition, PTUs possess a broader diffuse microphase boundary thickness compared to PUs. This can be due to the difference in the length distribution of the hard segment or soft segment and hard-soft segment compatibility [27, 32, 33]. Moreover, the phase mixing within domains for PTUs was smaller than for PUs, suggesting that a lower amount of hard segments (excess isocyanate blocks) are dissolved in the matrix or soft segments included in the hard segment domains [31]. Thus, we can state that the phase mixing within domains has a strong influence on the overall phase separation in PTU and PU elastomers.

Figure 5 shows the temperature dispersion of dynamic viscoelastic functions (dynamic storage modulus (E'), dynamic loss modulus (E''), and loss tangent (tan δ)) of the PTUs and PUs. The E' and tan δ inflection point were detected at approximately $-70\,°C$ due to α relaxation of the soft segment [34–36], which for PTUs is slightly lower than for PUs, indicating a stronger degree of microphase separation. This result corresponds well with the value obtained by DSC measurement. At approximately $-20\,°C$, a shoulder assigned to recrystallization of the soft segments was clearly observed for PTUs, which is consistent with a large exothermic peak in DSC. On the other hand, a shoulder that appears in PUs was smaller than in PTUs. As heating continues, a rubbery plateau was observed from 5 to 145 °C. The magnitude of E' at the rubbery plateau region for PTUs was slightly lower than for PUs. This is because
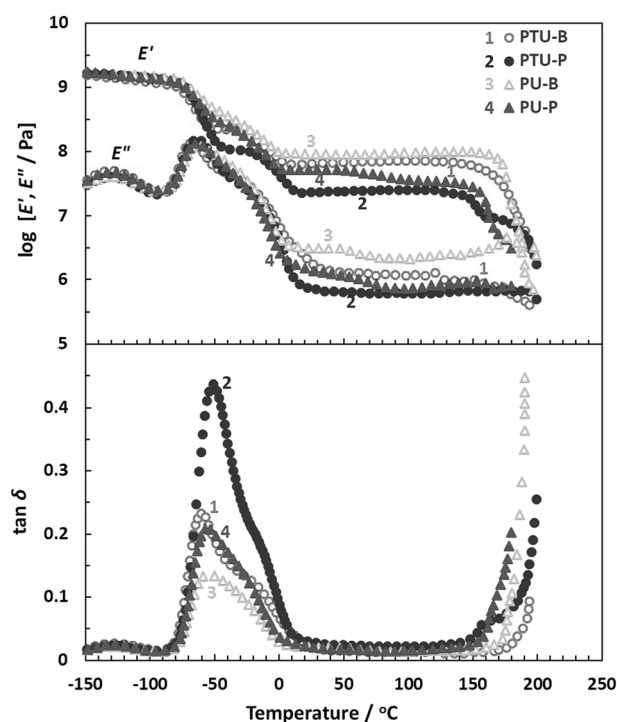

Fig. 5 E', E'', and tanδ-temperature relationship for the PTUs and PUs measured at 11 Hz

the ordering of the hard segment chains in PTUs is lower than in PUs. Therefore, the hard segment did not work well as physical crosslinking points in PTUs.

A decrease in the rubbery plateau was observed for PU with a PD-based chain extender, suggesting that the hard segment chains were not stable with increasing temperature. Thus, it seems reasonable to conclude that the effect of the chain extender on the mechanical properties for PU is stronger than for PTUs. Moreover, the terminal temperature of PTUs is lower than that of PUs with the same type of chain extender, with an additional weak plateau observed for PTUs, indicating a thermally less stable hard segment because of the lower ordering of the hard segment chains. This is very consistent with the $T_{m,H}$ obtained by DSC.

The physical properties of PTU and PU elastomers were evaluated with tensile testing. Figure 6 represents the stress–strain curves for PTUs and PUs, and Table 3 summarizes their mechanical properties. The Young's modulus for PTUs was slightly lower than for PUs. This trend corresponds well to the E' at the rubbery plateau region. This is because the hard segment chains ordering in PTUs is lower than in PUs, as was already mentioned above. The tensile strength difference for both PUs is greater than that for PTUs, indicating that the influence of the chain extender on the mechanical properties for PU is stronger than that for PTU.

Figure 7 shows a schematic representation of the microdomain structure of PTU and PU elastomers. The PTUs possess a stronger degree of overall phase separation, less phase mixing within domains, and a wider boundary thickness in comparison with PUs. On the other hand, the ordering and lamella thickness of the hard segment of PTUs is lower and smaller than for PUs. In addition, the effect of the chain extender on the microdomain structure and mechanical properties in PU is stronger than in PTU.
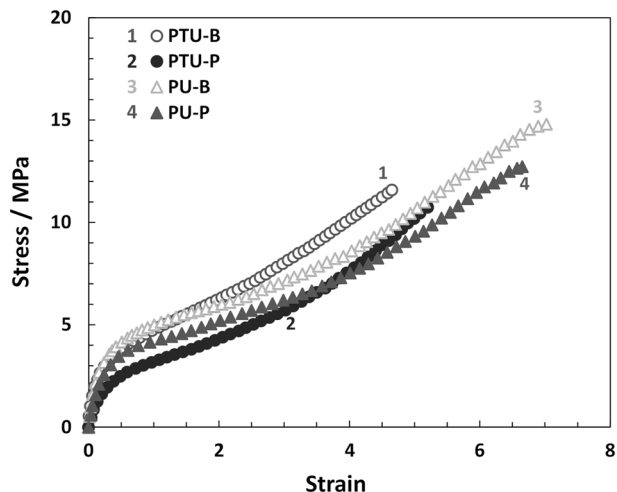

Fig. 6 Stress–strain curves for the PTU and PU elastomers measured at 25 °C

Table 3 Mechanical properties for the PTU and PU elastomers obtained from the stress–strain relations shown in Fig. 6

Elastomers	Young's modulus/ MPa	Tensile strength/ MPa	Strain at break
PTU-B	54.8 ± 5.7	11.6 ± 0.3	4.7 ± 0.3
PTU-P	28.1 ± 3.0	10.7 ± 0.4	5.2 ± 0.2
PU-B	61.4 ± 6.9	14.8 ± 0.6	7.1 ± 0.4
PU-P	41.7 ± 3.8	12.7 ± 0.5	6.7 ± 0.3

Conclusions

The microphase-separated structure and mechanical properties of 1,4-H_6XDI-based PTU elastomers were investigated. PTU and PU elastomers were prepared from PTMG, 1,4-H_6XDI and BDT, PDT, BD and PD. By using the dithiol chain extender instead of the diol, elastomers with a stronger degree of microphase separation and less domain mixing were produced. As a result, the PTU showed a better low temperature property, i.e., low T_g for the soft segment chain. However, since the ordering of the hard segment domains in the PTUs is lower than that for the PUs, they did not work well as physical crosslinking points, resulting in a mechanical property for PTUs that is comparable with PUs. Elastomers with a PD-based chain extender exhibited a lower degree of microphase-separated structure and mechanical property in comparison with elastomers with a BD-based chain extender. The influence of the methylene length of the chain extender on the microphase-separated structure and mechanical properties for PU is much stronger than that for PTU. PTU shows a weaker influence of the methylene length due to the stronger degree
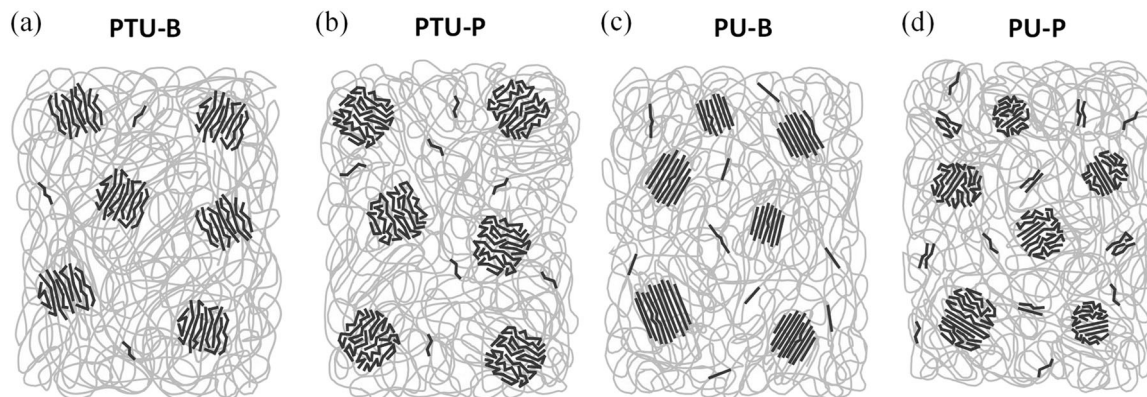

Fig. 7 Schematic representation of the microphase-separated structure for **a** PTU-B, **b** PTU-P, **c** PU-B, and **d** PU-P elastomers

of microphase separation and lower domain mixing compared to PU. It is expected that improvement of the mechanical properties of PTU can be achieved by fine-tuning the thermal history and hard segment content. The knowledge obtained in this study is useful for molecular structure design of PTUs for various applications.

Compliance with ethical standards

Conflict of interest The authors declare that they have no conflict of interest.

References

1. Kihara N, Endo T. Synthesis and properties of poly(hydroxyurethane)s. J Polym Sci. 1993;31:2765–73.
2. Tomita H, Sanda F, Endo T. Model reaction for the synthesis of polyhydroxyurethanes from cyclic carbonates with amines: substituent effect on the reactivity and selectivity of ring-opening direction in the reaction of five-membered cyclic carbonates with amine. J Polym Sci. 2001;39:3678–85.
3. Tomita H, Sanda F, Endo T. Structural analysis of polyhydroxyurethane obtained by polyaddition of bifunctional five-membered cyclic carbonate and diamine based on the model reaction. J Polym Sci. 2001;39:851–9.
4. Leitsch EK, Beniah G, Liu K, Lan T, Heath WH, Scheidt KA, et al. Nonisocyanate thermoplastic polyhydroxyurethane elastomers via cyclic carbonate aminolysis: critical role of hydroxyl groups in controlling nanophase separation. ACS Macro Lett. 2016;5:424–9.
5. Cao S, Li S, Li M, Xu L, Ding H, Xia J, et al. A thermal self-healing polyurethane thermoset based on phenolic urethane. Polym J. 2017;49:775–81.
6. Jang JY, Do JY. Synthesis and evaluation of thermoplastic polyurethanes as thermo-optic waveguide materials. Polym J. 2014;46:349–54.
7. Ohno A, Hayashi M, Takasu A. Synthesis of sulfone-containing non-ionic polyurethanes for electrophoretic deposition coating. Polym J. 2018;50:959–66.
8. Li W, Jiang X, Wu R, Wang W. Fast shape recovery by changing the grafting ratio in polyurethane/montmorillonite–poly(methyl methacrylate) composites. Polym J. 2017;49:263–71.
9. Lü C, Cui Z, Li Z, Yang B, Shen J. High refractive index thin films of ZnS/polythiourethane nanocomposites. J Mater Chem. 2003;13:526–30.
10. Tanaka M, Kuma S, Funaya M.Kobayashi S. Thiourethane-based optical material. Report No. US20050131203A1. 2005.
11. Li Q, Zhou H, Wicks DA, Hoyle CE, Magers DH, Mcalexander HR. Comparison of small molecule and polymeric urethanes, thiourethanes, and dithiourethanes: hydrogen bonding and thermal, physical, and mechanical properties. Macromolecules. 2009;42:1824–33.
12. Shin J, Matsushima H, Chan JW, Hoyle CE. Segmented polythiourethane elastomers through sequential thiol−ene and thiol−isocyanate reactions. Macromolecules. 2009;42:3294–301.
13. Rogulska M, Kultys A, Olszewska E. New thermoplastic poly(thiourethane-urethane) elastomers based on hexane-1, 6-diyl diisocyanate (HDI). J Therm Anal Calorim. 2013;114:903–16.
14. Fedurco M, Ribezzo M, Delfino A. Polymer with urethane or thiourethane units for use, in particular, as an adhesion primer for bonding metal to rubber. US 20160122460-A1. 2016.
15. Masunaga H, Ogawa H, Takano T, Sasaki S, Goto S, Tanaka T, et al. Multipurpose soft-material SAXS/WAXS/GISAXS beamline at SPring-8. Polym J. 2011;43:471–7.
16. Kojio K, Matsuo K, Motokucho S, Yoshinaga K, Shimodaira Y, Kimura K. Simultaneous small-angle X-ray scattering/wide-angle X-ray diffraction study of the microdomain structure of polyurethane elastomers during mechanical deformation. Polym J. 2011;43:692–9.
17. Coleman MM, Lee KH, Skrovanek DJ, Painter PC. Hydrogen bonding in polymers. 4. Infrared temperature studies of a simple polyurethane. Macromolecules. 1986;19:2149–57.
18. Nagai A, Ochiai B, Endo T. Observation of optical activity in polythiourethane obtained by the controlled cationic ring-opening polymerization of chiral cyclic thiourethane derived from serine. J Polym Sci. 2005;43:1554–61.
19. Ireni NG, Narayan R, Basak P, Raju K. Poly (thiourethane-urethane)-urea as anticorrosion coatings with impressive optical properties. Polymer. 2016;97:370–9.
20. Ireni NG, Karuppaiah M, Narayan R, Raju K, Basak P. TiO$_2$/Poly (thiourethane-urethane)-urea nanocomposites: anticorrosion materials with NIR-reflectivity and high refractive index. Polymer. 2017;119:142–51.
21. Lee HS, Wang YK, Hsu SL. Spectroscopic analysis of phase separation behavior of model polyurethanes. Macromolecules. 1987;20:2089–95.
22. Brunette C, Hsu S, Macknight W. Hydrogen-bonding properties of hard-segment model compounds in polyurethane block copolymers. Macromolecules. 1982;15:71–7.
23. Kojio K, Fukumaru T, Furukawa M. Highly softened polyurethane elastomer synthesized with novel 1, 2-bis (isocyanate) ethoxyethane. Macromolecules. 2004;37:3287–91.
24. Kojio K, Furukawa M, Nonaka Y, Nakamura S. Control of mechanical properties of thermoplastic polyurethane elastomers by restriction of crystallization of soft segment. Materials. 2010;3:5097–110.
25. Furukawa M, Mitsui Y, Fukumaru T, Kojio K. Microphase-separated structure and mechanical properties of novel polyurethane elastomers prepared with ether based diisocyanate. Polymer. 2005;46:10817–22.
26. Born L, Hespe H, Crone J, Wolf K. The physical crosslinking of polyurethane elastomers studied by X-ray investigation of model urethanes. Colloid Polym Sci. 1982;260:819–28.
27. Nozaki S, Masuda S, Kamitani K, Kojio K, Takahara A, Kuwamura G, et al. Superior properties of polyurethane elastomers synthesized with aliphatic diisocyanate bearing a symmetric structure. Macromolecules. 2017;50:1008–15.
28. Kojio K, Nakashima S, Furukawa M. Microphase-separated structure and mechanical properties of norbornane diisocyanate-based polyurethanes. Polymer. 2007;48:997–1004.
29. Blackwell J, Nagarajan M, Hoitink T. Structure of polyurethane elastomers: effect of chain extender length on the structure of MDI/diol hard segments. Polymer. 1982;23:950–6.

30. Vonk C. Investigation of non-ideal two-phase polymer structures by small-angle X-ray scattering. J Appl Crystallogr. 1973;6:81–6.
31. Bonart R, Müller EH. Phase separation in urethane elastomers as Judged by low-angle X-Ray scattering. II. Experimental Results. J Macromol Sci, Phys. 1974;10:345–57.
32. Koberstein JT, Stein RS. Small-angle X-ray scattering studies of microdomain structure in segmented polyurethane elastomers. J Polym Sci. 1983;21:1439–72.
33. Ophir Z, Wilkes GL. SAXS analysis of a linear polyester and a linear polyether urethane—interfacial thickness determination. J Polym Sci. 1980;18:1469–80.
34. Kojio K, Nakamura S, Furukawa M. Effect of side groups of polymer glycol on microphase-separated structure and mechanical properties of polyurethane elastomers. J Polym Sci. 2008;46:2054–63.
35. Takahara A, Tashita J, Kajiyama T, Takayanagi M. Effect of aggregation state of hard segment in segmented poly (urethaneureas) on their fatigue behavior after interaction with blood components. J Biomed Mater Res. 1985;19:13–34.
36. Kojio K, Furukawa M, Motokucho S, Shimada M, Sakai M. Structure− mechanical property relationships for poly (carbonate urethane) elastomers with novel soft segments. Macromolecules. 2009;42:8322–7.